Int J Appl Earth Obs Geoinformation 78 (2019) 77–85

Contents lists available at ScienceDirect

Int J Appl Earth Obs Geoinformation

journal homepage: www.elsevier.com/locate/jag

Improving the detection of wildfire disturbances in space and time based on indicators extracted from MODIS data: a case study in northern Portugal

Bruno Marcos[a,b,*], João Gonçalves[a,b], Domingo Alcaraz-Segura[c,d,e], Mário Cunha[b,f], João P. Honrado[a,b]

[a] Research Network in Biodiversity and Evolutionary Biology, Research Centre in Biodiversity and Genetic Resources (InBIO-CIBIO), Universidade do Porto, Campus Agrário de Vairão, Rua Padre Armando Quintas, 4485-661 Vairão, Portugal
[b] Faculdade de Ciências, Universidade do Porto, Rua Campo Alegre s/n, 4169-007 Porto, Portugal
[c] Dept. of Botany, Faculty of Sciences, University of Granada, Av. Fuentenueva, 18071 Granada, Spain
[d] iecolab. Interuniversitary Institute for Earth System Research (IISTA), University of Granada, Av. del Mediterráneo, 18006 Granada, Spain
[e] Andalusian Center for the Assessment and Monitoring of Global Change (CAESCG), Universidad de Almería, Crta. San Urbano, 04120 Almería, Spain
[f] Institute for Systems and Computer Engineering, Technology and Science (INESC TEC), Campus da Faculdade de Engenharia da Universidade do Porto, Rua Dr. Roberto Frias, Porto 4200-465, Portugal

ARTICLE INFO

Keywords:
Wildfire disturbance
Burned area mapping
Burn date estimation
Spectral indices
TCT
LST

ABSTRACT

Wildfires constitute an important threat to human lives and livelihoods worldwide, as well as a major ecological disturbance. However, available wildfire databases often provide incomplete or inaccurate information, namely regarding the timing and extension of fire events. In this study, we described a generic framework to compare, rank and combine multiple remotely-sensed indicators of wildfire disturbances, in order to not only select the best indicators for each specific case, as well as to provide multi-indicator consensus approaches that can be used to detect wildfire disturbances in space and time. For this end, we compared the performance of different remotely-sensed variables to discriminate burned areas, by applying a simple change-point analysis procedure on time-series of MODIS imagery for the northern half of Portugal, without external information (e.g. active fire maps). Overall, our results highlight the importance of adopting a multi-indicator consensus approach for mapping and detecting wildfire disturbances at a regional scale, that allows to profit from spectral indices capturing different aspects of the Earth's surface, and derived from distinct regions of the electromagnetic spectrum. Finally, we argue that the framework here described can be used: (i) in a wide variety of geographical and environmental contexts; (ii) to support the identification of the best possible remotely-sensed functional indicators of wildfire disturbance; and (iii) for improving and complementing incomplete wildfire databases.

1. Introduction

Worldwide, wildfires pose a major threat to a wide range of environmental, social, and economic assets. In the Mediterranean biome, wildfire activity has increased in the last decades (San-Miguel-Ayanz et al., 2013). Today, they constitute one of the major ecological disturbances as they can disrupt populations, communities and ecosystems, in terms of structure, composition, and function (Pickett and White, 1985). Indeed, fire (or disturbance regime) has been proposed not only as an Essential Climate Variable (ECV), but also as an Essential Biodiversity Variable (EBV) related to ecosystem function to assess biodiversity status (Pereira et al., 2013). There is thus a need to detect and characterize wildfire events in order to better understand how fire extent, frequency, and timing affect multiple environmental and socio-economic processes (Benali et al., 2016).

However, currently available fire databases may be hindered by errors, including coarse spatial resolutions, limited temporal extent, missing data, and unknown accuracy (e.g. ICNF, 2017). Furthermore, the costs of acquiring spatially comprehensive and consistent in-field data regarding wildfires (e.g. burn perimeters, ignition sources, deflagration time) can be high, as it is a time consuming and difficult process, and also because the allocated resources to it by land management authorities can highly fluctuate across time and space (Benali et al., 2016; Schroeder et al., 2016). There is thus a need to employ consistent frameworks to characterize wildfire disturbances that can help overcome those problems, by correcting or complementing the information provided by available fire databases.

In this context, an important contribution has been provided by

* Corresponding author: Campus Agrário de Vairão, Rua Padre Armando Quintas, 4485-661 Vairão, Portugal.
E-mail address: bruno.marcos@cibio.up.pt (B. Marcos).

https://doi.org/10.1016/j.jag.2018.12.003
Received 12 October 2018; Received in revised form 7 December 2018; Accepted 7 December 2018

Remote Sensing (RS) based on Earth Observation Satellites (EOS), which has particular utility for rapidly measuring, monitoring, and developing low-cost indicators for fire-related applications, with an increasing number of products being made available in recent years (Mouillot et al., 2014). As one of the sensors that currently provides frequent data with spectral bands appropriate for wildfire applications, the Moderate Resolution Imaging Spectroradiometer (MODIS) aboard the Terra and Aqua satellite platforms has been broadly used for fire applications. Although this sensor provides information at moderate to coarse spatial resolutions for wildfire disturbance mapping, it can be a valuable tool for monitoring, mainly at regional scales, due to its high data acquisition rate, wide availability of the datasets, and a data archive spanning almost two decades (Giglio et al., 2018; Justice et al., 2002).

RS-based approaches to map and detect wildfire disturbances can be categorized in one of two types (Joyce et al., 2009), namely: (i) active fires (e.g. MODIS Thermal Anomalies and Fires products MCD45 and MCD64, VIIRS NRT 375 Active Fire products); or (ii) burned areas (e.g. MODIS Burned Area products MOD14/MYD14/MCD14, Fire_cci Global Burned Area products). Detection of fire itself – active fires (AF) – consists in identifying thermal anomalies, usually at moderate to coarse spatial resolutions, but with high temporal frequency (e.g. daily), in order to detect phenomena that can be sometimes very concentrated in time, and do not account for the immediate effects of the fire on ecosystems directly (Chu and Guo, 2013; Lentile et al., 2006). In turn, detection of the short-term effects of fire events on the land surface – burned areas (BA) – type of approaches consists of mapping areas with burnt vegetation, by comparing pre- and post-fire reflectance information, and also against surrounding areas. As this uses optical and/or non-thermal infra-red data, it can be obtained at finer spatial scales, but often at lower temporal frequencies (Chu and Guo, 2013; Lentile et al., 2006), although this has been improving throughout the years. Finally, as this second type of approaches provides more direct observations of the effects of fire on the land surface (e.g. change in vegetation), rather than the physical phenomenon itself, they are more suitable for environmental applications that focus on biotic components (e.g. loss of biomass and/or habitats, water and nutrient availability), rather than abiotic components (e.g. gas emissions, pollution), and thus more fit to study post-fire responses of ecosystems to wildfire disturbances (Lentile et al., 2006).

In this context, several different variables extracted from time-series of satellite images (SITS), have been used for detecting wildfire disturbances, and their immediate effects on terrestrial ecosystems. Perhaps the most well-known of those are band ratios and normalized indices – sometimes referred to as vegetation indices (VI) or spectral indices (SI) – such as the Normalized Difference Vegetation Index (NDVI), the Enhanced Vegetation Index (EVI), or the Normalized Burn Ratio (NBR) (e.g. Moreno Ruiz et al., 2012; Veraverbeke et al., 2011). In a different approach, the variation in the LST/SI can be used for a wide range of applications related with disturbance events (e.g. Petropoulos et al., 2009). For instance, the MODIS Global Disturbance Index (MGDI; Mildrexler et al., 2009) uses the contrast between LST and EVI to map disturbances such as wildfires, with the underlying principle that LST decreases with an increase in vegetation density, given the greater latent heat transfer from increased evapotranspiration.

The Tasselled Cap Transformation (TCT; Lobser and Cohen, 2007) has also been previously used for the development of indicators of wildfire disturbances (e.g. Hilker et al., 2009). The three TCT main features – Brightness, Greenness, and Wetness – are SI but contain information on a wider portion of the electromagnetic spectrum, as more bands are used in their computation. These have been compared with a number of biophysical parameters, including albedo, amount of photosynthetically active vegetation and soil moisture, respectively (Mildrexler et al., 2009). Using these variables, Healey et al. (2005) and Thayn and Buss (2015) proposed a simple and weighted version, respectively, of a wildfire disturbance indicator, based on the principle that the Brightness feature increases after a fire, while the Greenness and the Wetness features decrease. On the other hand, as noted by Thayn and Buss (2015), in the period immediately after the fire event, the Brightness values actually decrease, since the burned areas are covered in charcoal and ash and thus are darker than the unburned areas. In a more recent study (Fornacca et al., 2018), TCT components were also shown to be useful for burn scar mapping, and for evaluating burn severity and post-fire recovery, from short- to long-term.

It is known that results can vary depending on spectral index and methods (Hislop et al., 2018). Therefore, in order to optimize accuracy of burned area detection algorithms, the best spectral indices (SI) should be selected accordingly (Fornacca et al., 2018). However, there is still uncertainty around which are the most essential variables for detecting and assessing wildfire disturbance, and their advantages and limitations (Hislop et al., 2018). In this study, we describe a generic framework to compare, rank and combine multiple remotely-sensed indicators of wildfire disturbances, in order to not only select the best indicators for each specific case, as well as to provide multi-indicator consensus approaches that can be used to detect wildfire disturbances in space and time. For this end, we compared the performance of different remotely-sensed variables to discriminate burned areas, by applying a simple change-point analysis procedure on time-series of MODIS imagery for the northern half of Portugal, without external information (e.g. active fire maps). In particular, we assessed which variables: (i) performed better in detecting and mapping wildfire occurrences at an annual temporal resolution; (ii) estimated better the date of occurrence (i.e. start of the wildfire); and (iii) could better complement missing information on available national fire databases, such as the one demonstrated for our study area. We finally discuss which variables may hold the greatest potential to contribute to assess and monitor wildfire disturbance, to be used as essential variables or to improve algorithms of wildfire disturbance detection and mapping.

2. Material and methods

2.1. Study area and data description

2.1.1. Study area

In order to illustrate our proposed framework, we used a study area that corresponds to the northern half of mainland Portugal, located in northwest Iberian Peninsula (Fig. 1). This region is among those with the highest incidence of wildfires across Europe (Barros and Pereira, 2014), both in terms of number of occurrences, and burned area (San-Miguel-Ayanz et al., 2017). It includes a strong climatic gradient (from humid Atlantic to dry Mediterranean), and a large diversity of bedrock formations, soil types, land cover and land use types (Carvalho-Santos et al., 2014; Vicente et al., 2013). Moreover, socio-economic drivers (e.g. land abandonment) and environmental conditions (e.g. steep slopes, terrain ruggedness, pyrophytic vegetation) contribute to a highly fire-prone region (Oliveira et al., 2012).

2.1.2. Spectral variables

Two MODIS products were downloaded and pre-processed using the *MODIStsp* R package (Busetto and Ranghetti, 2016), for all available dates between 2001 and 2016: (i) the Surface Reflectance (SR) product MOD09A1 (8-Day, L3, Global, 500), Collection 6 (Vermote, 2015); and (ii) the Land Surface Temperature (LST) and Emissivity product MOD11A2 (8-Day, L3, Global, 1-km), Collection 6 (Wan et al., 2015). Both products were re-projected to WGS84/UTM zone 29 N coordinate system, converted to GeoTIFF format, and re-sampled to 500 m using the nearest neighbor method, so that all raster data were at the same resolution.

In order to reduce noise that hinders time-series data we employed a filter based on the *Hampel* outlier identifier (Hampel, 1974, 1971) (window = 7 dates). This filter is considered robust, and efficient in identifying identifiers, as well as extremely effective in removing time-

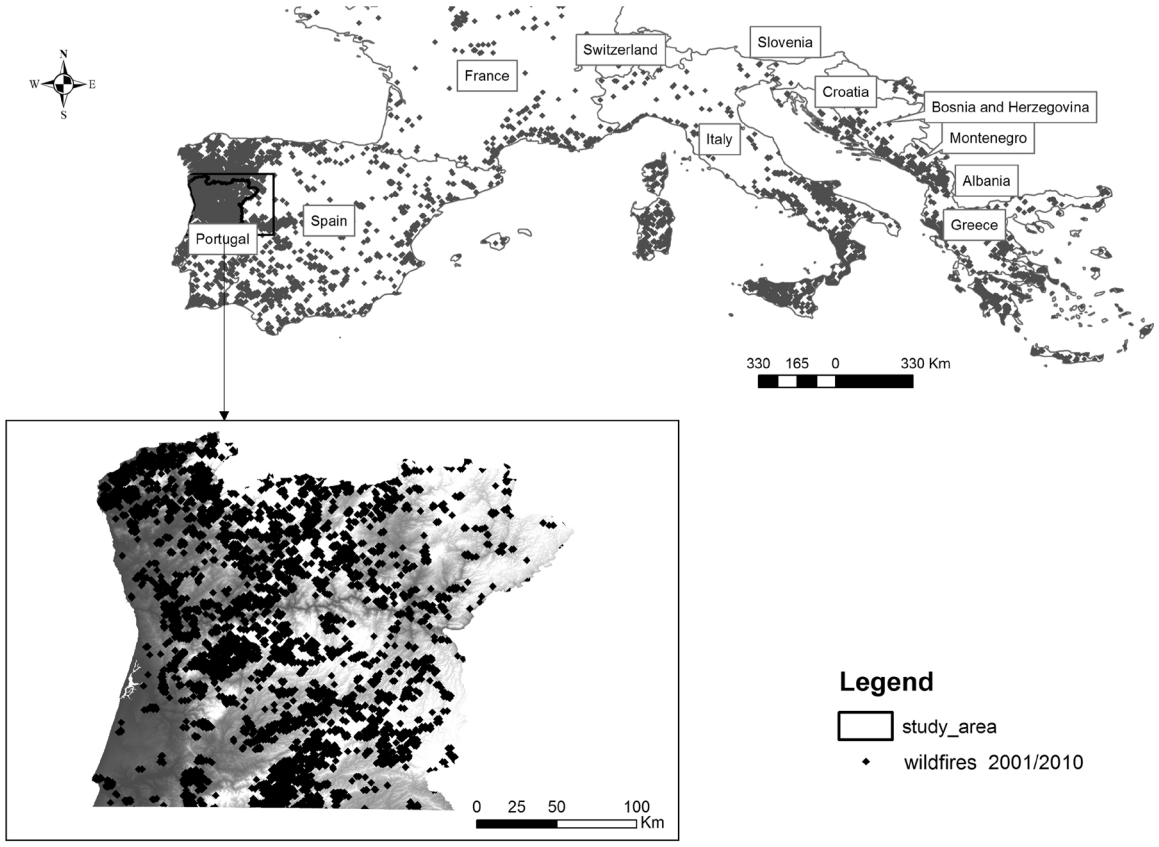

Fig. 1. The study area (bottom), in the context of southern Europe (top), with a representation of fire occurrences in the decade of 2001–2010 (dots), extracted from the European Forest Fire Information System (EFFIS).

series outliers (Pearson, 2002).

Then, the day-LST from the LST product was extracted and calibrated according to the guidelines described in the product's official documentation, and several spectral indices (SI) were computed by combining spectral bands from the SR product (Table 1), using GDAL (GDAL Contributors, 2017), and the rasterio Python package (Gillies et al., 2016). The final selection of variables was based on a literature review focused on potential indicators of wildfire disturbance, and includes SI that are commonly used in fire studies, such as: vegetation indices, "wetness" indices, fire-specific indices (e.g. Abade et al., 2015; Harris et al., 2011; Mildrexler et al., 2007; Schepers et al., 2014; Veraverbeke et al., 2012), and individual, or combinations of, tasseled cap features (e.g. Axel, 2018; Healey et al., 2005; Hermosilla et al., 2015; Patterson and Yool, 1998; Rogan and Yool, 2001; Santos et al., 2017). Finally, the Whittaker-Henderson smoother (Henderson, 1924; Whittaker, 1922) (with lambda = 2) was applied to these variables, in order to further reduce the remaining noise present in the data.

2.1.3. Reference fire datasets

The results from the wildfire disturbance detection were compared against three reference datasets, for the period between 2001 and 2016: the MODIS burned areas products (i) MCD45A1 (Collection 5.1; Roy et al., 2008), and (ii) MCD64A1 (Collection 6; Giglio et al., 2018), and (iii) the Portuguese national database of burned area polygons (ICNF, 2017).

The MCD45A1 algorithm uses a bidirectional reflectance distribution function (BRDF) model-based change detection approach to handle angular variations in the data, and analyzes the daily surface reflectance dynamics to locate rapid changes (Roy et al., 2008). It then uses that information to detect the approximate date of burning, and maps only the spatial extent of recent fires.

The MCD64A1 algorithm uses a burn sensitive VI, derived from shortwave infrared SR bands 5 and 7 with a measure of temporal texture, to create dynamic thresholds that are applied to the composite data. Compared to previous products (e.g. MCD45A1), MCD64A1 features a general improvement (reduced omission error) in burned area detection, including significantly better detection of small burns, as well as a modest reduction in burn-date temporal uncertainty (Giglio et al., 2018).

The Portuguese national database of burned area polygons, provided by the Portuguese national agency for nature conservation and forests (ICNF), contains annual fire perimeters from 1975 to 2017, with unknown accuracy, and heterogeneous characteristics – e.g. some perimeters were obtained from ground collected data, while others were derived from satellite imagery with different resolutions, such as Landsat and Sentinel; and only a small proportion of fires (i.e. ca. 11% of "big fires") have information on date of occurrence (see Supplementary materials for more information). The ICNF dataset was rasterized and re-projected to WGS84/UTM zone 29N, using GDAL/OGR v2.2.2 (GDAL Contributors, 2017), to match MODIS products.

The three reference datasets were converted to the same resolution as the spectral variables derived from MODIS. Then, fires with burned areas smaller than 100 ha (equivalent to 4 pixels) were excluded from the comparisons, in order to account for limitations of detectability inherent to the spatial scale of the MODIS products (van der Werf et al., 2017). This has also been the threshold used by Portuguese authorities to define "big fires" until 2013 (Ferreira-Leite et al., 2013) (later redefined to 500 ha).

2.2. Methodology

2.2.1. Detection of wildfire disturbances

Each selected spectral variable was used both on its own, and contrasted with LST, in a simple ratio (i.e. LST/index), and then

Table 1
List of spectral indices used in this study to derive wildfire disturbance indicators. The b1, b2, b3, b4, b5, b6, and b7 correspond to MODIS bands 1–7, with bandwidth ranges at 620–670 nm, 841–876 nm, 459–479 nm, 545–565 nm, 1230–1250 nm, 1628–1652 nm, and 2105–2155 nm, respectively.

Index	Designation	Formula
NDVI	Normalized Difference Vegetation Index	(b2 − b1)/(b2 + b1)
EVI2	Two-band Enhanced Vegetation Index	2.5 × (b2 − b1)/(b2 + (2.4 × b1) + 1)
NDWI	Normalized Difference Water Index	(b4 − b6)/(b4 + b6)
LSWI	Land Surface Water Index	(b2 − b6)/(b2 + b6)
NBR	Normalized Burn Ratio	(b2 − b7)/(b2 + b7)
TCTb	Tasseled Cap Brightness	(0.4395 × b1) + (0.5945 × b2) + (0.2460 × b3) + (0.3918 × b4) + (0.3506 × b5) + (0.2136 × b6) + (0.2678 × b7)
TCTg	Tasseled Cap Greenness	(−0.4064 × b1) + (0.5129 × b2) + (−0.2744 × b3) + (−0.2893 × b4) + (0.4882 × b5) + (−0.0036 × b6) + (−0.4169 × b7)
TCTw	Tasseled Cap Wetness	(0.1147 × b1) + (0.2489 × b2) + (0.2408 × b3) + (0.3132 × b4) + (−0.3122 × b5) + (−0.6416 × b6) + (−0.5087 × b7)
TCTbg	Tasseled Cap Brightness + Greenness	(TCTb + TCTg)/2
TCTgw	Tasseled Cap Greenness + Wetness	(TCTg + TCTw)/2
TCTbw	Tasseled Cap Brightness + Wetness	(TCTb + TCTw)/2
TCTbgw	Tasseled Cap Brightness + Greenness + Wetness	(TCTb + TCTg + TCTw)/3

normalized using *Z*-scores normalization, pixel-wise, as: $Z = (x - \mu)/\sigma$, where 'x' is the original value, 'μ' is the time-series average, and 'σ' is the time-series standard deviation, giving a total of 24 indicators. In order to minimize the effects of both long-term and seasonal variation on each indicator time-series, as well as to highlight abrupt changes such as those associated with wildfire disturbance events, we decomposed the normalized time-series using a Seasonal-Trend decomposition procedure based on the LOESS smoother (STL; Cleveland et al., 1990). This was done with the 's.window' and 't.window' parameters both equal to 47, as it corresponds to the next odd number from the frequency of the time series, i.e. 46 images per year, and the 'robust' parameter set as TRUE. The LOESS procedure decomposes time-series into 'trend', 'seasonal' and 'remainder' components. The resulting 'remainder' component was used as disturbance indicator, as it corresponds to the detrended and de-seasonalized time-series, and thus contains the non-periodical variations, as well as any remaining noise (which was greatly reduced in previous steps).

Tukey's fences (Tukey, 1977) were used for detecting wildfire disturbances, by identifying which peaks could be considered outliers, i.e. peaks farther away than 'k' times (in this case $k = 3$, for 'far away' outliers) the interquartile range from the nearest quartile were considered as positive detections, as those represent the values that most likely correspond to severe outliers within each pixel-wise time-series' (Tukey, 1977). This approach also allows to obtain estimates of the period of occurrence of the wildfire disturbance event, i.e. in which 8-day composite it was detected. These computations were undertaken using the R statistical programming environment (R Core Team, 2018).

2.2.2. Evaluation of indicators' performance

In order to evaluate the performance of each indicator to detect and map wildfire disturbances, at the annual temporal resolution, the following single-class performance measures were extracted from the confusion matrices (Fawcett, 2006): Sensitivity (i.e. true positive rate) or Producer's Accuracy (i.e. the complement of omission error), Specificity (i.e. true negative rate), User's Accuracy (i.e. the complement of commission error), Overall Accuracy, and Cohen's Kappa. Both the values and their respective confidence intervals for Kappas were estimated using bootstrap with 10,000 repetitions, in order to test the statistical significance of the differences between the indicators' burned areas maps. For simplification purposes, the detections resulting from the wildfire disturbance indicators, and from the two reference datasets obtained from MODIS products were compared against the national reference database.

The results of the temporal estimations from the 24 indicators were compared against the reference datasets, for the fires for which occurrence dates were available, within the 2012–2016 period. This allowed to evaluate the indicators in terms of both temporal precision (i.e. dispersion in the temporal estimations) – through standard deviation (SD) and median absolute deviation (MAD), and interquartile range (IQR), and temporal accuracy (i.e. degree of success in estimating dates of occurrence) – using mean absolute error (MAE) and median absolute error (MDAE), and mean (MB) and median bias (MDB). Based on this, ten of the indicators were excluded. However, four of those were reconsidered, as they exhibited high precision, only with a systematic error of only one composite. Those four indicators were then corrected for systematic lag (i.e. a temporal shift of one composite was applied), and added to the list of indicators, elevating the final count of indicators considered to 28.

Finally, based on the performance metrics, the wildfire disturbance indicators were ranked, which was used to find the "best" occurrence date estimate for each pixel, i.e. the date estimate given by the highest ranked indicator for which there was a positive detection. This, along with the median of the date estimates from the indicators that were not excluded by this process, provided two estimates of date of occurrence, for each pixel. Then, these estimates, as well as the dates given by the two reference datasets from MODIS burned area products, were

Table 2
Performance of burned area mapping, on an annual basis (2001–2016), for the selected indicators, compared to the Portuguese national fire polygons database. MODIS burned area products MCD45 and MCD64 were also compared, and their performance results are also presented (as "mcd45_v51" and "mcd64_v6", respectively). Note that indicators here are presented with lower case, to denote the difference between each indicator and the index, indices, or product in which it was based on (indicator names with underscore were based in ratios, as described in the text). Both estimates for Kappas and their respective confidence intervals (CI) were obtained by bootstrapping with 10,000 repetitions.

Indicator	Formula	Sensitivity	Specificity	Producer's accuracy	User's accuracy	Overall accuracy	Kappa	Kappa CI
mcd45_v51	–	0.929	0.992	0.929	0.991	0.960	0.921	0.918–0.926
mcd64_v6	–	0.922	0.992	0.922	0.992	0.957	0.915	0.910–0.919
lst_tbgw	LST/TCTbgw	**0.962**	0.988	**0.962**	0.987	**0.975**	**0.950**	**0.946–0.952**
lst_evi2	LST/EVI2	0.956	0.985	0.956	0.985	0.971	0.941	0.938–0.945
lst_tctg	LST/TCTg	0.949	0.975	0.949	0.974	0.962	0.923	0.920–0.928
lst_tcbw	LST/TCTbw	0.927	0.991	0.927	0.990	0.959	0.918	0.912–0.920
lst_tcbg	LST/TCTbg	0.889	0.994	0.889	0.994	0.941	0.883	0.878–0.888
lst_ndvi	LST/NDVI	0.878	0.989	0.878	0.988	0.934	0.867	0.863–0.873
tctg	TCTg	0.845	0.993	0.845	0.992	0.919	0.837	0.832–0.843
nbri	NBR	0.817	0.992	0.817	0.991	0.905	0.809	0.805–0.817
tbgw	TCTbgw	0.753	0.996	0.753	0.994	0.874	0.749	0.743–0.756
evi2	EVI2	0.716	0.993	0.716	0.991	0.855	0.710	0.703–0.717
lst_tctb	LST/TCTb	0.662	0.997	0.662	**0.996**	0.830	0.660	0.653–0.668
lst_nbri	LST/NBR	0.753	0.889	0.753	0.872	0.821	0.643	0.637–0.652
ndvi	NDVI	0.596	0.991	0.596	0.985	0.794	0.587	0.579–0.595
tcbg	TCTbg	0.588	0.996	0.588	0.993	0.792	0.584	0.578–0.593
lswi	LSWI	0.556	0.996	0.556	0.993	0.776	0.552	0.545–0.560
tcbw	TCTbw	0.441	0.998	0.441	0.994	0.719	0.438	0.432–0.447
tcgw	TCTgw	0.421	0.710	0.421	0.992	0.709	0.418	0.410–0.426
lst_lswi	LST/LSWI	0.536	0.710	0.536	0.649	0.623	0.246	0.238–0.258
tctb	TCTb	0.166	**0.998**	0.166	0.990	0.582	0.164	0.159–0.170
lst_tcgw	LST/TCTgw	0.512	0.641	0.512	0.588	0.577	0.154	0.140–0.161
lst_tctw	LST/TCTw	0.051	0.997	0.051	0.937	0.524	0.047	0.045–0.051
ndwi	NDWI	0.041	0.985	0.041	0.724	0.513	0.025	0.022–0.029
lst_ndwi	LST/NDWI	0.020	0.998	0.020	0.910	0.509	0.018	0.016–0.020
tctw	TCTw	0.019	0.995	0.019	0.794	0.507	0.014	0.012–0.017

Values in bold highlight the highest values in each column.

extracted and aggregated to match the geometry of the "big fire" polygons (i.e. above 100 ha) of the national reference dataset, including all burned area polygons both with and without prior information of the date of occurrence, for the period of 2001–2016. This was done in order to provide estimates of the dates of occurrence of the wildfire disturbance events, to complement the information previously available in the national reference dataset, from only a portion (ca. 11%) of the "big fire" polygons for years between 2012 and 2016, to all "big fire" polygons of the dataset, from 2001 to 2016 (see Supplementary material for more information).

3. Results and discussion

3.1. Burned area mapping performance

Mapping accuracies of annual burned areas, when compared to the national fire reference dataset, were generally high across all indicators (Overall Accuracy ≥ 0.75; Kappa ≥ 0.50), with non-overlapping confidence intervals for Kappa estimates in most cases (Table 2; Fig. 2). Only the ones based on 'wetness' indices (except LSWI) attained lower performance (Table 2). The highest values for Specificity and User's Accuracy were achieved for the indicators based on TCTb and the LST/TCTb ratio, respectively, while for the remaining performance metrics, the highest values all resulted from the indicator derived from the LST/TCTbgw ratio (Fig. 2).

In comparison, MODIS Burned Areas products achieved very good accuracy results, with all performance metrics scoring above 0.92. Although it uses an updated and improved algorithm, the Collection 6 product (MCD64) obtained slightly lower accuracies than the Collection 5.1 product (MCD45) for our study area (Table 2).

Overall, mapping accuracies, at the annual temporal resolution, resulted in better performances when using indicators based on LST/SI ratios, in comparison with the indicators using the same indices but without the contrast with LST. This is in line with results from previous studies (e.g. Mildrexler et al., 2009, 2007) where the coupling of LST and SI, particularly in LST/SI ratios, substantially improved the detection of changes, as the two variables in the ratio respond to different biophysical processes, thereby complementing the information content of one another.

When compared with indicators based on more widely-used SI (e.g. NDVI, EVI2, NBR), indicators based on tasseled cap features, and tasseled cap features combinations, resulted in improved accuracies, confirming the importance of considering their use for mapping burned areas (Arnett et al., 2014; Healey et al., 2005; Santos et al., 2017). This could be because tasseled cap features use a wider portion of the electromagnetic spectrum (including visible, near infrared and shortwave infrared) than other SI, which may provide more complete pictures of wildfire disturbance processes (Fornacca et al., 2018).

3.2. Temporal estimates of wildfire disturbances

The performance of estimates of wildfire occurrence dates, using 8-day composites from the period 2012–2016, yielded diverse results across different indicators, when compared to the dates available in the national fire dataset (Fig. 3). Of a total of 28 indicators considered, 16 of those achieved very good results in terms of both temporal precision and temporal accuracy, with values of median absolute deviations (MAD), median absolute errors (MDAE), and median biases (MDB) around zero, while interquartile ranges (IQR) were between 0 and 1 composites of 8 days. Values of mean bias (MB), standard deviation (SD) and mean absolute deviance (MAE) were used to differentiate and rank the indicators, with values for the two MODIS reference datasets generally worse than the top 16 indicators (Table 3). The remaining 12 indicators were excluded from the final estimates extracted for the national fire database, since they had overall lower scores for temporal precision and accuracy, ranking bellow the two MODIS reference datasets (used for comparison).

The indicators 'tcbg', 'tbgw', 'tctg' and 'evi2' were ranked, in that

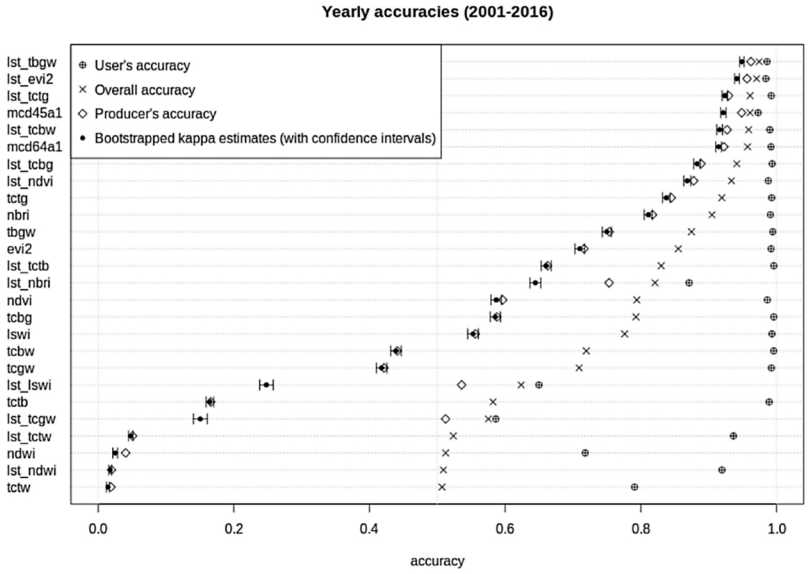

Fig. 2. Dot chart representing the yearly burned area mapping accuracy measures for 2001–2016, for each one of the indicators used, as well as the MODIS burned area products MCD45 and MCD64 (as "mcd45_v51" and "mcd64_v6", respectively), compared to the national fire database. Bootstrapped estimates for Kappa are shown with their respective confidence intervals.

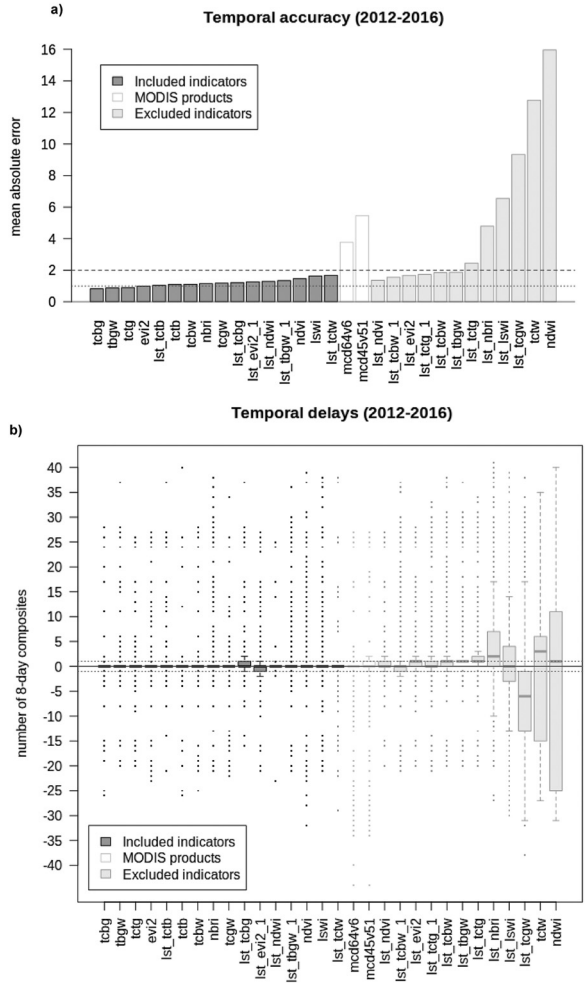

Fig. 3. Temporal accuracies (a) and delays (i.e. errors) (b) of the estimates of wildfire occurrence date, compared to the Portuguese national fire database. The horizontal lines mark specially remarkable values for the mean absolute errors: 1 (dots) and 2 (dashes). Besides the estimates for the indicators, the comparison of the dates given by the MODIS Burned Area products MCD45 and MCD64, in comparison with the national database, are shown as "mcd45v51" and "mcd64v6", respectively. Additional information such as sample sizes is presented in Table 3.

Table 3
Performance statistics of temporal delays, in relation to the national reference dataset. The values are expressed in number of 8-day composites, as this is the maximum precision for wildfire date estimates that the input data allows. The indicators that were corrected for a systematic lag of one 8-day composite are denoted with the suffix "_1". Results for the MODIS Burned Area products MCD45 and MCD64 area also given here, as "mcd45v51" and "mcd64v6", respectively.

Rank	Indicator	*n*	MAD	MDAE	IQR	SD	MAE	MDB	MB
1	tcbg	2851	0	0	0	**3.89**	**0.82**	0	+0.39
2	tbgw	3462	0	0	0	3.99	0.87	0	+0.43
3	tctg	3976	0	0	0	4.02	0.90	0	+0.40
4	evi2	3599	0	0	0	4.24	0.99	0	+0.46
5	lst_tctb	3325	0	0	0	4.25	1.04	0	+0.70
6	tctb	909	0	0	0	4.68	1.09	0	+0.21
7	tcbw	2121	0	0	0	4.56	1.10	0	+0.44
8	nbri	3798	0	0	0	4.56	1.15	0	+0.63
9	tcgw	2430	0	0	0	4.58	1.18	0	+0.49
10	lst_tcbg	4218	0	0	1	4.15	1.21	0	+0.91
11	lst_evi2_1	4537	0	0	1	4.16	1.26	0	+0.32
12	lst_ndwi	241	0	0	0	4.87	1.29	0	+0.71
13	lst_tbgw_1	4533	0	0	0	4.32	1.34	0	+0.60
14	ndvi	3268	0	0	0	5.23	1.46	0	+0.80
15	lswi	2530	0	0	0	5.46	1.63	0	+0.95
16	lst_tctw	336	0	0	0	5.39	1.67	0	−0.20
17	mcd64v6	4659	0	0	0	9.72	3.77	0	−2.37
18	mcd45v51	4637	0	0	1	11.49	5.46	0	−3.76
19	lst_ndvi	4091	1.48	1	1	4.10	1.36	0	+1.05
20	lst_tcbw_1	4353	1.48	1	1	4.79	1.55	0	+0.55
21	lst_evi2	4537	0	1	1	4.16	1.67	+1	+1.32
22	lst_tctg_1	4484	1.48	1	1	4.35	1.73	0	+1.20
23	lst_tcbw	4353	1.48	1	1	4.79	1.84	+1	+1.55
24	lst_tbgw	4533	0	1	0	4.32	1.86	+1	+1.60
25	lst_tctg	4484	1.48	1	1	4.35	2.44	+1	+2.20
26	lst_nbri	3824	2.97	2	7	6.46	4.79	+2	+4.37
27	lst_lswi	2876	4.45	3	7	9.86	6.55	0	**+0.04**
28	lst_tcgw	2844	8.90	8	12	10.47	9.34	−6	−6.04
29	tctw	155	19.27	14	21	14.79	12.77	+3	−2.41
30	ndwi	658	23.72	16	36	18.76	15.95	+1	−2.99

order, in the first four places, being the indicators with the lowest values for SD and MAE, and low values of MB (i.e. below 4.25, 1, and 0.50, respectively). Here, "mcd45_v51" and "mcd64_v6" correspond to the MODIS burned area products MCD45 and MCD64, respectively. On the other hand, the majority of the indicators based on an LST/SI ratio were among the ones excluded.

In perspective, when estimating dates of occurrence, indicators that included at least one TCT component – but not LST – showed better

overall results of temporal precision and accuracy. This contrasts with the results from the annual mapping performance, suggesting that including both TCT features and LST may help improve burned area mapping, however, the inclusion of LST may result in less accurate and less precise burn date estimation. Also, it must be noted that the indicators that included all three TCT components, with or without LST, (i.e. 'tbgw' and 'lst_tbgw') ranked in one of the top two positions for both wildfire disturbance mapping and detection, while, to the best of our knowledge, these indicators have not been previously used for those specific purposes.

Together, these results reinforce that no single indicator is the best for all purposes simultaneously, pointing to a trade-off situation, in which the "best" (i.e. top ranked) indicators for burned area mapping, and the best ones for estimating the respective time of occurrence, may not be necessarily the same. This suggests that, for those purposes, adopting a multi-indicator approach may be advantageous in order to obtain the best possible results, in that different indicators may complement the potential that each have, while compensating each other's drawbacks, to detect and map wildfire disturbances.

3.3. Complementing fire databases gaps

For the final estimations of the date of occurrence of wildfire disturbance events, inter-comparison of density distributions of the dates given by all the five datasets compared (Fig. 4) showed an overall high degree of similarity between the different datasets (see Supplementary material for more detailed information). This suggests a high congruence between the date estimates given by the different datasets, and thus a reasonable confidence level in the date estimates obtained for the remaining polygons of the national fire database, assuming the similarities between datasets would hold.

The top ranked indicator (i.e. 'tcbg') provided estimates for 41.4% of the complete set of "big fire" polygons of burned areas from the national fire database, while the indicators ranked in second and third (i.e. 'tbgw' and 'tctg') contributed with further 16.1% and 12.4%, respectively (Fig. 5). Although the indicators ranked next provided estimates for relatively low percentages of fire polygons, three other indicators contributed to estimate dates for additional percentages of "big fire" polygons above 5% (Table 4).

In comparison, when each of the same indicators were used independently, rather than in a rank-based sequence, the ones that were able to provide estimates for the highest percentages of fire polygons, were 'lst_evi2' and 'lst_tbgw' (after systematic error correction), with 95.1% each, while the top three indicators achieved percentages between 59.8% (for 'tctb') and 83.4% (for 'tctg').

Our results further highlight the potential of TCT components to be used to estimate date of occurrence of wildfire disturbances, and – together with the results from burned area mapping – for their application in fire studies using remotely-sensed data. This, as pointed out in other studies (e.g. Fornacca et al., 2018), indicates that, since these SI use the information of all seven spectral bands in the optical-NIR-SWIR regions, they may possess enhanced capabilities to capture more aspects of ecosystem functioning change due to fires, especially when combined. In turn, this suggests that TCT components constitute a more complete, comprehensive and compact package of base information to study wildfire disturbance processes than the more commonly used SI, making them a particularly interesting option for fire-related monitoring (e.g. ECV, EBV).

All in all, for the purposes of systematically selecting the best spectral indices to derive indicators of wildfire disturbances, extracted from satellite images time series, and for complementing the information already available in fire databases, the framework here presented is generic enough to be applicable to other study areas. This is because the signal patterns that allow for the detection of such disturbances within satellite images time series, as well as the spectral responses of vegetation to wildfire disturbance, tend to be similar across different biomes, vegetation types, and climatic regimes (e.g. Hope et al., 2012; Lanorte et al., 2014; Leon et al., 2012).

4. Conclusions

Despite the vast amount of remote-sensing studies that assess wildfires, there is still a need for protocols to systematically select the best indicators at the local or regional scale to develop algorithms that detect, map and assess such disturbances, and to complement the information on existing databases. For tackling this, in this study, we analyzed and compared several indices, derived from time series of MODIS images, for the assessment and monitoring of wildfire disturbances. Moreover, this work contributed to improve the selection of the best indicators, derived from remotely sensed indices, with potential to improve existing information in national fire databases, for ecological and environmental applications, at a regional scale. This was accomplished by proposing a multi-indicator consensus approach which allowed to profit from spectral indices capturing different aspects of the Earth's surface, and derived from distinct regions of the electromagnetic spectrum. Finally, although satellite data with coarse spatial resolution was used here, the same principles (and a similar framework) could be used employing satellite time series data from recent or upcoming platforms with higher spatial resolution, but still high temporal frequency (e.g. Sentinel-2 or PRISMA sensors).

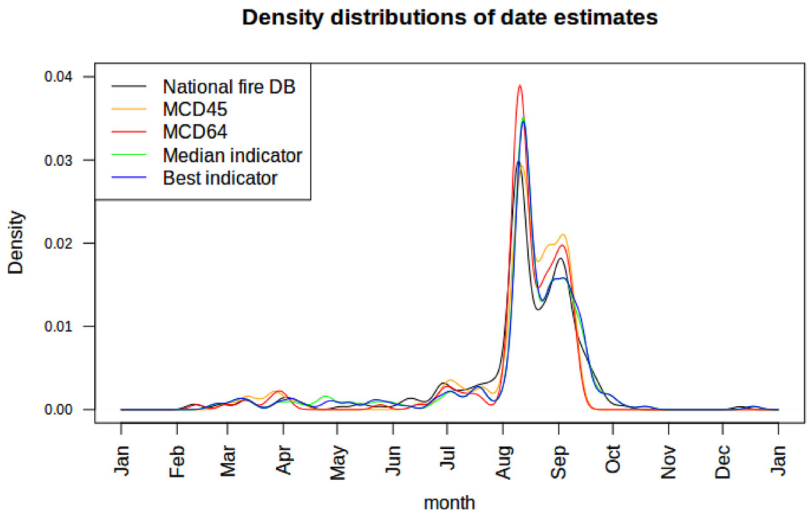

Fig. 4. Density distributions of dates from all the five datasets compared (i.e. reference – National fire DB, MCD45 and MCD64, and date estimates from the 'Median' and 'Best' indicators). For comparability purposes, only the dates available for the same polygons as the ones with date information on the national fire database were plotted.

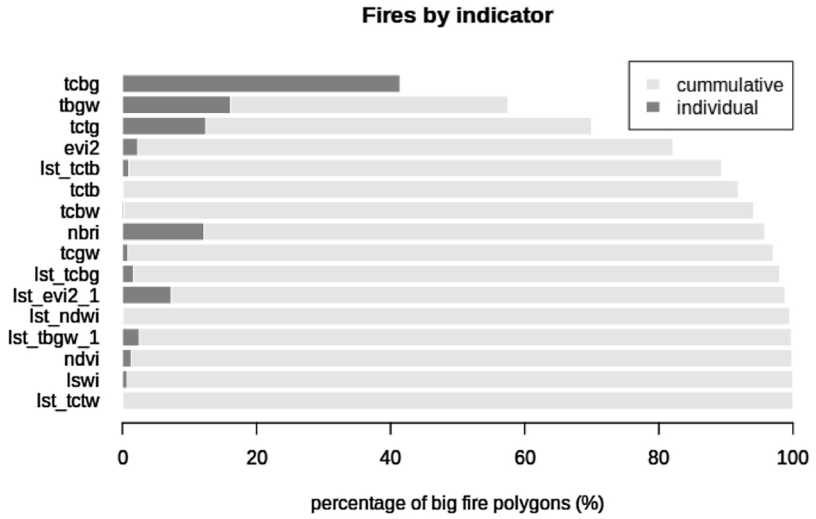

Fig. 5. Percentage of burned area polygons of the Portuguese national fire database (with area above 100 ha) for which each indicator was considered the "best" (i.e. the top ranked) indicator. For more information, including sample sizes, see Table 4.

Table 4
Results from final extraction of fire occurrence dates, using the best ranked indicator for each pixel, for all the burned area polygons of the national fire database above 100 ha (i.e. "big fires").

Rank	Indicator	No. pixels	% pixels	No. polygons	% polygons	Accumulated % polygons
1	tcbg	2851	59.8%	833	41.4%	41.4%
2	tbgw	3462	72.6%	324	16.1%	57.5%
3	tctg	3976	83.4%	250	12.4%	69.9%
4	evi2	3599	75.5%	245	2.3%	72.2%
5	lst_tctb	3325	69.7%	146	0.9%	73.2%
6	tctb	909	19.1%	50	0.1%	73.3%
7	tcbw	2121	44.5%	46	0.2%	73.5%
8	nbri	3798	79.6%	33	12.2%	85.7%
9	tcgw	2430	51.0%	26	0.8%	86.5%
10	lst_tcbg	4218	88.4%	19	1.6%	88.1%
11	lst_evi2_1	4537	95.1%	16	7.3%	95.4%
12	lst_ndwi	241	5.1%	14	0.1%	95.5%
13	lst_tbgw_1	4533	95.1%	6	2.5%	98.0%
14	ndvi	3268	68.5%	2	1.3%	99.3%
15	lswi	2530	53.1%	2	0.7%	100.0%
16	lst_tctw	336	7.0%	1	0.0%	100.0%
17	mcd64_v6	4659	97.7%	–	–	
18	mcd45_51	4637	97.2%	–	–	

Acknowledgements

Bruno Marcos and J. F. Gonçalves were financially supported by the Portuguese Foundation for Science and Technology (FCT), through PhD Grants SFRH/BD/99469/2014 and SFRH/BD/90112/2012, respectively, funded by the Ministry of Education and Science, and the European Social Fund, within the 2014-2020 EU Strategic Framework. D. Alcaraz-Segura received funding from JC2015-00316 grant and CGL2014-61610-EXP.

Appendix A. Supplementary data

Supplementary data associated with this article can be found, in the online version, at doi:10.1016/j.jag.2018.12.001.

References

Abade, N., Júnior, O., Guimarães, R., de Oliveira, S., 2015. Comparative analysis of MODIS time-series classification using support vector machines and methods based upon distance and similarity measures in the Brazilian Cerrado-Caatinga boundary. Remote Sens. 7, 12160–12191. https://doi.org/10.3390/rs70912160.

Arnett, J.T.T.R., Coops, N.C., Gergel, S.E., Falls, R.W., Baker, R.H., 2014. Detecting stand-replacing disturbance using RapidEye Imagery: a tasseled cap transformation and modified disturbance index. Can. J. Remote Sens. 40, 1–14. https://doi.org/10.1080/07038992.2014.899878.

Axel, A., 2018. Burned area mapping of an escaped fire into tropical dry forest in western Madagascar using multi-season Landsat OLI Data. Remote Sens. 10, 371. https://doi.org/10.3390/rs10030371.

Barros, A.M.G., Pereira, J.M.C., 2014. Wildfire selectivity for land cover type: does size matter? PLoS One 9, e84760. https://doi.org/10.1371/journal.pone.0084760.

Benali, A., Russo, A., Sá, A., Pinto, R., Price, O., Koutsias, N., Pereira, J., 2016. Determining fire dates and locating ignition points with satellite data. Remote Sens. 8, 326. https://doi.org/10.3390/rs8040326.

Busetto, L., Ranghetti, L., 2016. MODIStsp: an R package for automatic preprocessing of MODIS Land Products time series. Comput. Geosci. 97, 40–48. https://doi.org/10.1016/j.cageo.2016.08.020.

Carvalho-Santos, C., Honrado, J.P., Hein, L., 2014. Hydrological services and the role of forests: conceptualization and indicator-based analysis with an illustration at a regional scale. Ecol. Complex. 20, 69–80. https://doi.org/10.1016/j.ecocom.2014.09.001.

Chu, T., Guo, X., 2013. Remote Sensing techniques in monitoring post-fire effects and patterns of forest recovery in Boreal forest regions: a review. Remote Sens. 6, 470–520. https://doi.org/10.3390/rs6010470.

Cleveland, R.B., Cleveland, W.S., McRae, J.E., Terpenning, I., 1990. STL: a seasonal-trend decomposition procedure based on loess. J. Off. Stat. https://doi.org/citeulike-article-id:1435502.

Fawcett, T., 2006. An introduction to ROC analysis. Pattern Recognit. Lett. 27, 861–874. https://doi.org/10.1016/j.patrec.2005.10.010.

Ferreira-Leite, F., Lourenço, L., Bento-Gonçalves, A., 2013. Large forest fires in mainland Portugal, brief characterization. Méditerranée 53–65. https://doi.org/10.4000/mediterranee.6863.

Fornacca, D., Ren, G., Xiao, W., 2018. Evaluating the best spectral indices for the

detection of burn scars at several post-fire dates in a mountainous region of northwest Yunnan, China. Remote Sens. 10, 1196. https://doi.org/10.3390/rs10081196.
GDAL Contributors, 2017. GDAL – Geospatial Data Abstraction Library: Version 1.11.2.
Giglio, L., Boschetti, L., Roy, D.P., Humber, M.L., Justice, C.O., 2018. The Collection 6 MODIS burned area mapping algorithm and product. Remote Sens. Environ. 217, 72–85. https://doi.org/10.1016/j.rse.2018.08.005.
Gillies, S., et al., 2016. Rasterio: Geospatial Raster I/O for Python Programmers.
Hampel, F.R., 1974. The influence curve and its role in robust estimation. J. Am. Stat. Assoc.
Hampel, F.R., 1971. A general qualitative definition of robustness. Ann. Math. Stat. 42, 1887–1896.
Harris, S., Veraverbeke, S., Hook, S., 2011. Evaluating spectral indices for assessing fire severity in Chaparral ecosystems (Southern California) using MODIS/ASTER (MASTER) airborne simulator data. Remote Sens. 3, 2403–2419. https://doi.org/10.3390/rs3112403.
Healey, S., Cohen, W., Zhiqiang, Y., Krankina, O., 2005. Comparison of Tasseled Cap-based Landsat data structures for use in forest disturbance detection. Remote Sens. Environ. 97, 301–310. https://doi.org/10.1016/j.rse.2005.05.009.
Henderson, R., 1924. A new method of graduation. Trans. Actuar. Soc. Am. 25, 29–40.
Hermosilla, T., Wulder, M.A., White, J.C., Coops, N.C., Hobart, G.W., 2015. Regional detection, characterization, and attribution of annual forest change from 1984 to 2012 using Landsat-derived time-series metrics. Remote Sens. Environ. 170, 121–132. https://doi.org/10.1016/j.rse.2015.09.004.
Hilker, T., Wulder, M.A., Coops, N.C., Seitz, N., White, J.C., Gao, F., Masek, J.G., Stenhouse, G., 2009. Generation of dense time series synthetic Landsat data through data blending with MODIS using a spatial and temporal adaptive reflectance fusion model. Remote Sens. Environ. 113, 1988–1999. https://doi.org/10.1016/j.rse.2009.05.011.
Hislop, S., Jones, S., Soto-Berelov, M., Skidmore, A., Haywood, A., Nguyen, T., 2018. Using Landsat spectral indices in time-series to assess wildfire disturbance and recovery. Remote Sens. 10, 460. https://doi.org/10.3390/rs10030460.
Hope, A., Albers, N., Bart, R., 2012. Characterizing post-fire recovery of fynbos vegetation in the Western Cape Region of South Africa using MODIS data. Int. J. Remote Sens. 33, 979–999. https://doi.org/10.1080/01431161.2010.543184.
ICNF, 2017. Forest fires – Geographical information. http://www.icnf.pt/portal/florestas/dfci/inc/info-geo (accessed 01.10.17).
Joyce, K.E., Belliss, S.E., Samsonov, S.V., McNeill, S.J., Glassey, P.J., 2009. A review of the status of satellite remote sensing and image processing techniques for mapping natural hazards and disasters. Prog. Phys. Geogr. 33, 183–207. https://doi.org/10.1177/0309133309339563.
Justice, C., Giglio, L., Korontzi, S., Owens, J., Morisette, J., Roy, D., Descloitres, J., Alleaume, S., Petitcolin, F., Kaufman, Y., 2002. The MODIS fire products. Remote Sens. Environ. 83, 244–262. https://doi.org/10.1016/S0034-4257(02)00076-7.
Lanorte, A., Lasaponara, R., Lovallo, M., Telesca, L., 2014. Fisher–Shannon information plane analysis of SPOT/VEGETATION Normalized Difference Vegetation Index (NDVI) time series to characterize vegetation recovery after fire disturbance. Int. J. Appl. Earth Obs. Geoinf. 26, 441–446.
Lentile, L.B., Holden, Z.A., Smith, A.M.S., Falkowski, M.J., Hudak, A.T., Morgan, P., Lewis, S.A., Gessler, P.E., Benson, N.C., 2006. Remote sensing techniques to assess active fire characteristics and post-fire effects. Int. J. Wildl. Fire 15, 319. https://doi.org/10.1071/WF05097.
Leon, J.R.R., van Leeuwen, W.J.D., Casady, G.M., Leon, J.R.R., van Leeuwen, W.J.D., Casady, G.M., 2012. Using MODIS-NDVI for the modeling of post-wildfire vegetation response as a function of environmental conditions and pre-fire restoration treatments. Remote Sens. 4, 598–621. https://doi.org/10.3390/rs4030598.
Lobser, S.E., Cohen, W.B., 2007. MODIS Tasselled Cap: land cover characteristics expressed through transformed MODIS data. Int. J. Remote Sens. 28, 5079–5101. https://doi.org/10.1080/01431160701253303.
Mildrexler, D.J., Zhao, M., Running, S.W., 2009. Testing a MODIS Global Disturbance Index across North America. Remote Sens. Environ. 113, 2103–2117. https://doi.org/10.1016/j.rse.2009.05.016.
Mildrexler, D.J., Zhao, M.S., Heinsch, F.A., Running, S.W., 2007. A new satellite-based methodology for continental-scale disturbance detection. Ecol. Appl. 17, 235–250. https://doi.org/10.1890/1051-0761(2007)017[0235:ANSMFC]2.0.CO;2.
Moreno Ruiz, J.A., Riaño, D., Arbelo, M., French, N.H.F., Ustin, S.L., Whiting, M.L., 2012. Burned area mapping time series in Canada (1984–1999) from NOAA-AVHRR LTDR: a comparison with other remote sensing products and fire perimeters. Remote Sens. Environ. 117, 407–414. https://doi.org/10.1016/j.rse.2011.10.017.
Mouillot, F., Schultz, M.G., Yue, C., Cadule, P., Tansey, K., Ciais, P., Chuvieco, E., 2014. Ten years of global burned area products from spaceborne remote sensing—a review: analysis of user needs and recommendations for future developments. Int. J. Appl. Earth Obs. Geoinf. 26, 64–79. https://doi.org/10.1016/j.jag.2013.05.014.
Oliveira, S.L.J., Pereira, J.M.C., Carreiras, J.M.B., Abaimov, S., Turcotte, D., Shcherbakov, R., Rundle, J., Díaz-Delgado, R., Lloret, F., Pons, X., Fisher, J., Loneragan, W., Dixon, K., Delaney, J., Veneklaas, E., Grissino-Mayer, H., Heinselman, M., Johnson, E., Gutsell, S., Kraaij, T., Lloret, F., Marí, G., McCarthy, M., Gill, A., Bradstock, R., Moritz, M., Moritz, M., Keeley, J., Johnson, E., Shaffner, A., Moritz, M., Moody, T., Miles, L., Smith, M., Valpine, P., de Nunes, M., Vasconcelos, M., Pereira, J., Dasgupta, N., Alldredge, R., Rego, F., O'Donnell, A., Boer, M., McCaw, W., Grierson, P., Pereira, M., Trigo, R., DaCamara, C., Pereira, J., Leite, S., Polakow, D., Dunne, T., Trigo, R., Pereira, J., Pereira, M., Mota, B., Calado, T., DaCamara, C., Santo, F., Vázquez, A., Moreno, J., 2012. Fire frequency analysis in Portugal (1975–2005), using Landsat-based burnt area maps. Int. J. Wildl. Fire 21, 48. https://doi.org/10.1071/WF10131.
Patterson, M.W., Yool, S.R., 1998. Mapping fire-induced vegetation mortality using Landsat Thematic Mapper Data: a comparison of linear transformation techniques. Remote Sens. Environ. 65, 132–142. https://doi.org/10.1016/S0034-4257(98)00018-2.
Pearson, R.K., 2002. Outliers in process modeling and identification. IEEE Trans. Control Syst. Technol. 10, 55–63. https://doi.org/10.1109/87.974338.
Pereira, H.M., Ferrier, S., Walters, M., Geller, G.N., Jongman, R.H.G., Scholes, R.J., Bruford, M.W., Brummitt, N., Butchart, S.H.M., Cardoso, A.C., Coops, N.C., Dulloo, E., Faith, D.P., Freyhof, J., Gregory, R.D., Heip, C., Höft, R., Hurtt, G., Jetz, W., Karp, D.S., McGeoch, M.A., Obura, D., Onoda, Y., Pettorelli, N., Reyers, B., Sayre, R., Scharlemann, J.P.W., Stuart, S.N., Turak, E., Walpole, M., Wegmann, M., 2013. Ecology. Essential biodiversity variables. Science 339, 277–278. https://doi.org/10.1126/science.1229931.
Petropoulos, G., Carlson, T.N., Wooster, M.J., Islam, S., 2009. A review of Ts/VI remote sensing based methods for the retrieval of land surface energy fluxes and soil surface moisture. Prog. Phys. Geogr. 33, 224–250. https://doi.org/10.1177/0309133309338997.
Pickett, S.T., White, P.S., 1985. The Ecology of Natural Disturbance and Patch Dynamics. Academic Press.
R Core Team, 2018. R: A Language and Environment for Statistical Computing. Version 3.4.
Rogan, J., Yool, S.R., 2001. Mapping fire-induced vegetation depletion in the Peloncillo Mountains. Int. J. Remote Sens. 22, 3101–3121. https://doi.org/10.1080/01431160152558279.
Roy, D.P., Boschetti, L., Justice, C.O., Ju, J., 2008. The collection 5 MODIS burned area product—global evaluation by comparison with the MODIS active fire product. Remote Sens. Environ. 112, 3690–3707. https://doi.org/10.1016/j.rse.2008.05.013.
San-Miguel-Ayanz, J., Durrant, T., Boca, R., Libertà, G., Branco, A., de Rigo, D., Ferrari, D., Maianti, P., Vivancos, T.A., Schulte, E., Loffler, P., 2017. Forest Fires in Europe, Middle East and North Africa 2016. Luxembourg. https://doi.org/10.2760/66820.
San-Miguel-Ayanz, J., Moreno, J.M., Camia, A., 2013. Analysis of large fires in European Mediterranean landscapes: lessons learned and perspectives. For. Ecol. Manage. 294, 11–22. https://doi.org/10.1016/j.foreco.2012.10.050.
Santos, F., Dubovyk, O., Menz, G., 2017. Monitoring forest dynamics in the Andean Amazon: the applicability of breakpoint detection methods using Landsat time-series and genetic algorithms. Remote Sens. 9, 68. https://doi.org/10.3390/rs9010068.
Schepers, L., Haest, B., Veraverbeke, S., Spanhove, T., Borre, J., Goossens, R., 2014. Burned area detection and burn severity assessment of a Heathland Fire in Belgium using airborne imaging spectroscopy (APEX). Remote Sens. https://doi.org/10.3390/rs6031803.
Schroeder, W., Oliva, P., Giglio, L., Quayle, B., Lorenz, E., Morelli, F., 2016. Active fire detection using Landsat-8/OLI data. Remote Sens. Environ. 185, 210–220. https://doi.org/10.1016/j.rse.2015.08.032.
Thayn, J.B., Buss, K.L., 2015. Monitoring fire recovery in a tallgrass prairie using a weighted disturbance index. GISci. Remote Sens.
Tukey, J.W., 1977. Exploratory Data Analysis. Pearson.
van der Werf, G.R., Randerson, J.T., Giglio, L., van Leeuwen, T.T., Chen, Y., Rogers, B.M., Mu, M., van Marle, M.J.E., Morton, D.C., Collatz, G.J., Yokelson, R.J., Kasibhatla, P.S., 2017. Global fire emissions estimates during 1997–2016. Earth Syst. Sci. Data 9, 697–720. https://doi.org/10.5194/essd-9-697-2017.
Veraverbeke, S., Hook, S., Hulley, G., 2012. An alternative spectral index for rapid fire severity assessments. Remote Sens. Environ. 123, 72–80. https://doi.org/10.1016/j.rse.2012.02.025.
Veraverbeke, S., Lhermitte, S., Verstraeten, W.W., Goossens, R., 2011. Evaluation of pre/post-fire differenced spectral indices for assessing burn severity in a Mediterranean environment with Landsat Thematic Mapper. Int. J. Remote Sens. 32, 3521–3537. https://doi.org/10.1080/01431161003752430.
Vermote, E., 2015. MOD09A1 MODIS/Terra Surface Reflectance 8-Day L3 Global 500m SIN Grid V006. NASA EOSDIS L. Process. DAAC.
Vicente, J.R., Fernandes, R.F., Randin, C.F., Broennimann, O., Gonçalves, J., Marcos, B., Pôças, I., Alves, P., Guisan, A., Honrado, J.P., 2013. Will climate change drive alien invasive plants into areas of high protection value? An improved model-based regional assessment to prioritise the management of invasions. J. Environ. Manage. 131, 185–195.
Wan, Z., Hook, S., Hulley, G., 2015. MOD11A2 MODIS/Terra Land Surface Temperature/Emissivity 8-Day L3 Global 1km SIN Grid V006. NASA EOSDIS L. Process. DAAC.
Whittaker, E.T., 1922. On a new method of graduation. Proc. Edinburgh Math. Soc. 41, 63–75.